Proceeding of the IEEE
International Conference on Robotics and Biomimetics
Dali, China, December 2019

A Novel Visual Odometer Assisted Pose Tracking Method for Mobile Robots

Rupeng Yuan, Fuhai Zhang , Ying Zhu and Yili Fu
The State Key Laboratory of Robotics and System
Harbin Institute of Technology
Harbin 150001, China
zfhhit@hit.edu.cn

***Abstract* - Pose tracking is very crucial for robot's autonomous navigation. LIDAR based pose tracking algorithms are widely used due to its high cost-effective advantage. However these methods are likely to give back wrong result if the environment is blocked by the obstacles. In this paper, a visual odometer assisted pose tracking method is proposed to increase the robustness of pose tracking. Statistical index is introduced to evaluate the samples' score of LIDAR based pose tracking. If the result is not credible, the result of visual odometer will compensate the error along the maximum error direction. The experiment shows that the proposed method is able to track the robot correctly if the environment is blocked by obstacles.**

Index Terms – Navigation; Pose tracking; Visual odometer;

I. INTRODUCTION

Localization is one of the most important capacities for mobile robots. Generally speaking, the purposes of localization are as follows: to globally locate a robot and to dynamically track one. Global localization[1] is often used to give an initial pose, or to solve the kidnapping problems. In actual application, however, the initial pose of a robot is often given in advance. Therefore, the need for global localization is not quite urgent. Pose tracking[2] however, is often used to dynamically and continuously locate a robot, which is very crucial in industrial realm. There are quite a few sensors available to track a robot. LIDARs[3][4] and cameras[5][6] are the most commonly used sensors, due to their high cost-effective advantages.

The localization algorithms using LIDARs are usually probability based. The Monte Carlo localization method is the most classic algorithm[7][8]. A variety of improvements have been made to the original Monte Carlo localization. The basic Monte Carlo localization may converge prematurely if the robot is located in a symmetrical environment[9]. A pose tracking method using progressive scan matching[10] is proposed to increase time efficiency and pose tracking accuracy. The LIDAR based pose tracking (LBPT) can track a robot well if the environment is not sheltered, however the method may fail to give back accurate result if the environment is severely blocked by obstacles.

The localization algorithms using cameras, generally known as visual odometer, are usually graph based. The graph based methods are generally solved using G2O[11] and ISAM[12] to increase computationally efficiency. The PTAM[13] method was proposed by Klein and Murray. The method uses parallel thread for pose tracking and mapping. The method can be used in small-scale augmented reality. Also, some algorithms can directly use pixel values to minimize optical flow errors. DTAM[14] uses dense visual information to track a robot. The algorithm needs real-time operation of GPU. Engel[15] uses semi-dense, even sparse visual information to track a robot, which only requires real-time operation of CPU.

In this paper, a novel visual odometer assisted pose tracking (VOAPT) method is introduced to increase the robustness of pose tracking of LIDAR based pose tracking. VOAPT integrates LIDAR and camera's information and enhanced the performance of pose tracking by determining the direction of pose tracking error of LIDAR based localization, and compensating the error along the direction. The experiments shows that VOAPT is able to track a robot with accuracy and robustness.

II. POSE ESTIMATION OF VISUAL ODOMETER

A. Search and matching of land mark features

Visual odometer uses landmarks to calculate poses. As the landmark is the projection of ORB feature points in three-dimensional space, each landmark has an ORB feature descriptor. The similarity between the two landmarks is described by the Hamming distance of their ORB feature descriptor.

$$dist_{Hamming} = \sum_{i=1}^{n} descriptor_m[i] \oplus descriptor_n[i] \quad (1)$$

In (1) $dist_{Hamming}$ denotes the Hamming distance between the road mark m and the road mark n. $descriptor_m$ and $descriptor_n$ are feature descriptors of two landmarks.

The violent matching is suitable for initial two-frame matching as well as re-localization and the motion-based matching is suitable for matching after initialization.

When the pose T_w^l of the current image in the world and the pose T_w^b of the previous image in the world are known, the velocity T_{vel} between two frames can be obtained:

$$T_{vel} = T_w^l \times T_b^w \quad (2)$$

T_b^w is the pose transformation from the world to the previous frame. Because of the high sampling frequency of the camera, the range of change between the current frame and the previous frame is also near T_{vel}. If the coordinate of the previous frame in the world is T_w^l, the coordinate of the current frame in the world is approximately T_w^n:

$$T_w^n = T_{vel} \times T_w^l \quad (3)$$

978-1-7281-6321-5/19//$31.00 ©2019 IEEE

After T_w^n is calculated, the coordinate of land mark $P_{ci} = [x_{ci}, y_{ci}, z_{ci}]^T$ in previous frame is $P_{ci}{}' = [x_{ci'}, y_{ci'}, z_{ci'}]^T$, the coordinate of $P_{ci}{}'$ in the image is (u_l, v_l):

$$P_{ci}{}' = T_l^w \times T_w^n \times P_{ci} \tag{4}$$

$$\begin{cases} u_l = f_x \cdot \dfrac{x_{ci}{}'}{z_{ci}{}'} + c_x \\ v_l = f_x \cdot \dfrac{y_{ci}{}'}{z_{ci}{}'} + c_y \end{cases} \tag{5}$$

In (5), T_l^w is the transformation from world to previous frame. Let the searching radius be r. With (u_l, v_l) as the center and r as the radius, feature points can be found from the image of the previous frame.

After retrieving all the ORB features from two images, PnP algorithm is used to estimate the pose of inter-frame cameras. In order to improve the stability and reliability of the algorithm, RANSAC algorithm should be introduced to reduce the impact of mismatching on the results. So far, the pose of the camera can be correctly calculated and the pose of the robot is uniquely determined by coordinate transformation.

B. Updating and Maintenance of Local Maps

The pose estimation using ORB feature points between two frames is easy to lose because of the lack of prior information. In order to ensure higher computational efficiency and smaller storage space, the size of local maps should be maintained at a certain size, so it is necessary to continue filtering key frames. If most of the landmarks in a key frame in a local map cannot be observed from a larger observation angle, the key frame needs to be deleted.

Let the number of key frames in local map is N_m, the number of landmarks in i^{th} keyframe is $N_c^{[i]}$. As T_w^n is known, the coordinate of current frame in the world is $coor_0^w = [x_0^c, y_0^c, z_0^c]^T$. The transformation from the world to the current frame is T_w^n. The coordinate of the j^{th} landmark defined in the i^{th} keyframe can be transformed into the current frame $coor_{ij}^c = [x_n, y_n, z_n]^T$, which can further be used to calculate the coordinate in the current image $[u_n, v_n]^T$:

$$\begin{cases} coor_{ij}^c = T_n^w \times coor_{ij}^w \\ u_n = \dfrac{f_x \times x_n}{z_n} + c_x \\ v_n = \dfrac{f_y \times y_n}{z_n} + c_y \end{cases} \tag{6}$$

If $[u_n, v_n]^T$ is located inside the image, then the landmark $coor_{ij}^w$ can be observed by the current frame. After that, it is also necessary to determine that the observed landmark is in the middle of the image. The vector from the landmark in the world coordinate system to the origin of the current frame is $\overrightarrow{d^w} = coor_{ij}^w - coor_0^w$. The visual angle θ_{view} from which the landmark is observed is:

$$\theta_{view} = \cos^{-1}\left(\frac{\overrightarrow{d^w} \cdot coor_{ij}^c}{\left\|\overrightarrow{d^w}\right\| \cdot \left\|coor_{ij}^c\right\|}\right) \tag{7}$$

If $\theta_{view} \geq \theta_{lim}$, then the landmark can be properly observed. θ_{lim} is the minimum observation angle. The number of landmark that can properly observed in i^{th} keyframe is $N_{seen}^{[i]}$. The current frame wouldn't be kept unless the ratio of $N_{seen}^{[i]}/N_c^{[i]}$ is above threshold.

III. Abnormal localization and localization control

A. The mathematical analysis of pose tracking samples

The mathematical analysis of the samples of LBPT can determine whether the current pose tracking result is trustworthy or not. Due to the existence of environmental occlusion, robot model error, sensor noise and data rounding error, the robot pose tracking results will inevitably fluctuate.

At time t, sampling-based LIDAR localization method generates n samples, and each sample use posterior probability to represent possible pose of robot. The posterior probability of i^{th} sample is:

$$p_i(x_i|z_t, m), 1 < i \leq n \tag{8}$$

In (8), x_i is the pose of the sample, z_t is the measurement at time t, m is the current grid map. The posterior probability distribution of each sample satisfies the definition of probability density function:

$$\sum_{i=1}^{n} p_i(x_i|z_t, m) = 1 \tag{9}$$

In order to evaluate the quality of single pose tracking results, a normalized score S_i' is needed to satisfy the definition of probability density function. Let the score of the i^{th} sample be S_i, then:

$$\begin{cases} S_i' = p_i(x_i|z_t, m) \\ S_i' = \dfrac{S_i}{\sum_{i=1}^{n} S_i} \end{cases} \tag{10}$$

The analysis of sample score is represented by box chart. A typical box chart can be seen in Fig.1(b). A box chart contains the maximum V_{max}, upper quartile V_{uq}, medium, lower quantile V_{lq} and the minimum V_{min} of the current pose tracking result.

Fig.1(a) shows the score distribution of pose tracking samples. The box chart can clearly reflect the discrete degree of each pose tracking sample, the data centralized area and the upper and lower bounds, so as to quantitatively give the evaluation of the current location.

As it is difficult to evaluate the results of a calculation comprehensively with single statistical indexes such as maximum, minimum and median of each pose tracking score, and the score of the sample is also related to the grid map. With the different environment and the limitation of the sensor's range, the score of each measurement sample will be quite different. Therefore, the proposed method requires the use of composite indicators to evaluate the pose tracking samples. The composite indicator C_s is consisted of maximum, Range-median difference and Range-quantile difference ratio.

1) The maximum V_{max}:

The maximum value represents the score of the optimal sample, and the larger the value, the higher the degree of fit between the LIDAR endpoint and the grid map, so the maximum value can be used as one of the composite indicators.

2) Range-median difference D_s:

Range-median difference reflects the dispersion degree of samples. In sample scoring of pose tracking, dispersion degree can reflect the accuracy of current localization. The higher the dispersion degree is, the more likely the maximum sample is to obtain the optimal pose. The Range-median D_s is:

$$\mathrm{D_s} = \mathrm{V_{max}} - \mathrm{V_{lq}} - \mathrm{V_{med}} \tag{11}$$

3) Range-quantile difference ratio $\mathbf{R_s}$:

The difference between the upper quartile and the lower quartile in the box chart can reflect the range of the dense area of the data. The larger the ratio, the more corresponding the maximum scoring value is. The more likely the sample is to be in the correct position. The Range-quantile difference ratio $\mathrm{R_s}$ is:

$$\mathrm{R_s} = \frac{\mathrm{V_{max}} - \mathrm{V_{lq}}}{\mathrm{V_{uq}} - \mathrm{V_{lq}}} \tag{12}$$

The composite indicator C_s can be represented as:

$$\mathrm{C_s} = (\mathrm{V_{max}} \geq \mathrm{V_{th1}}) \wedge (\mathrm{D_s} \geq \mathrm{V_{th2}}) \wedge (\mathrm{R_s} \geq \mathrm{V_{th3}}) \tag{13}$$

In (13), $\mathrm{V_{th1}}$, $\mathrm{V_{th2}}$ and $\mathrm{V_{th3}}$ are three threshold for each component of composite indicator C_s. The pose tracking result given by odometer is $\mathrm{P}_{odom} = (x_{odom}, y_{odom}, \theta_{odom})^T$. If $\mathrm{C_s} \neq 0$ then, the LIDAR based localization will correct the robot pose.

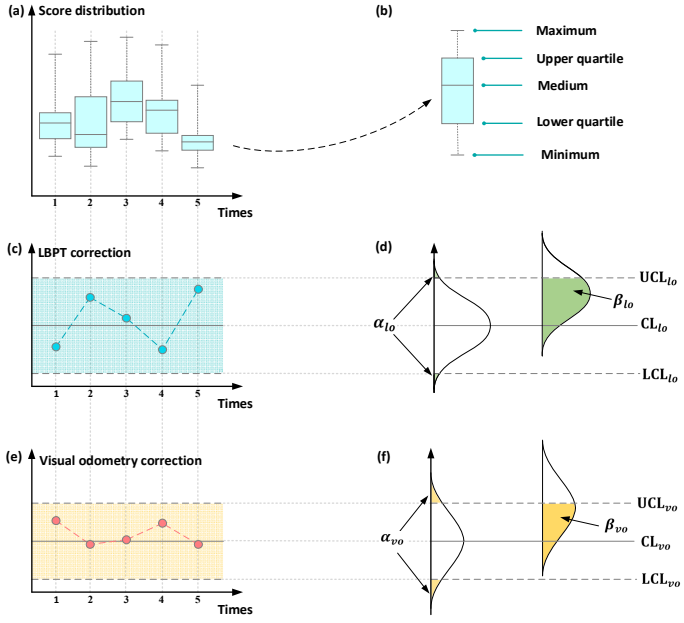

Fig. 1. Distribution of sample score and correction in normal operation

The correction R_{lo} obtained by each operation relative to the odometer is shown in the Fig.1(c). The average of correction is μ_{lo}, the standard deviation is σ_{lo}, then:

$$\begin{cases} UCL_{lo} = \mu_{lo} + 3\sigma_{lo} \\ CL_{lo} = \mu_{lo} \\ LCL_{lo} = \mu_{lo} - 3\sigma_{lo} \end{cases} \tag{14}$$

In (14), UCL_{lo}, CL_{lo} and LCL_{lo} are the upper control limit, central line and lower control limit of correction R_{lo}. Therefore, if the correction R_{lo} is between the control upper and lower limit, then the result is trustworthy.

Each time the composite index C_s is met, the correction of visual odometer to the odometer is R_{vo}, as shown in Fig.1(c). The average is μ_{vo} and the standard deviation is σ_{vo}, then:

$$\begin{cases} UCL_{vo} = \mu_{vo} + 3\sigma_{vo} \\ CL_{vo} = \mu_{vo} \\ LCL_{vo} = \mu_{vo} - 3\sigma_{vo} \end{cases} \tag{15}$$

In (15), UCL_{vo}, CL_{vo} and LCL_{vo} are the upper control limit, central line and lower control limit of correction R_{vo}. Therefore, if the correction R_{vo} is between the control upper and lower limit, then the result is trustworthy.

According to the composite indicator C_s, correction R_{lo} and correction R_{vo}, the credibility criteria $\mathrm{T_s}$ can be represented as

$$\mathrm{T_s} = (LCL_{lo} \leq R_{lo} \leq UCL_{lo}) \vee (LCL_{vo} \leq R_{vo} \leq UCL_{vo}) \tag{16}$$

If $\mathrm{T_s} = 1$, then the pose tracking is normal, the fluctuation of results is accidental. Otherwise, the result is abnormal, the direction of error should be further investigated and corrected.

B. Maximum error direction recognition and control

When the pose tracking results of LIDAR based localization fluctuate abnormally due to environmental occlusion or sensor errors, it is necessary to determine the direction of the maximum positioning error, and compensate the error in the direction by using visual odometer information to reduce the impact of abnormal fluctuations on the robot's pose tracking.

Samples involved in maximum error direction recognition in single pose tracking are sample index sets I_s whose score value is greater than the upper quartile:

$$I_s = \left\{ i \middle| \mathrm{V_{uq}} \leq S_i^{'} \leq \mathrm{V_{max}}, 1 \leq i \leq n \right\} \tag{17}$$

$\forall i \in I_s$, the correction of sample pose relative to odometer pose is $P_i = \left(x_i, y_i, \theta_i\right)^T$, the optimal sample is $P_{best} = \left(x_{best}, y_{best}, \theta_{best}\right)^T$.

The optimal translational correction of samples is $T_{best} = \left(x_{best}, y_{best}\right)^T$. Only when the heading angle of the optimal sample satisfies the (18), can the corrected displacement error direction of the sample be analysed and T_{best} be optimized.

$$\frac{\sum_{i=1}^{n} (\theta_{best} - \theta_i)^2}{n} \leq \theta_{lim}^2 \tag{18}$$

In (18), θ_{lim} is the maximum allowable error of heading angle. When the deviation of heading angle is not too large, principal component analysis (PCA) can be used to determine the maximum error direction of sample displacement correction. For $\forall i \in I_s$, the removing-mean coordinate $\left(x_i^{'}, y_i^{'}\right)^T$ of $\left(x_i, y_i\right)^T$ is:

$$\begin{cases} x_i^{'} = x_i - \dfrac{\sum_{i=1}^{n} x_i}{n} \\ y_i^{'} = y_i - \dfrac{\sum_{i=1}^{n} y_i}{n} \end{cases} \tag{19}$$

The removing-mean random variable on x-axis $\mathrm{X}^{'} = \left\{x_1^{'}, x_2^{'} \cdots x_n^{'}\right\}$ and on y-axis can be obtained through (19). Therefore, the covariance matrix is:

$$M_{cov} = \begin{pmatrix} cov\left(\mathrm{X}^{'}, \mathrm{X}^{'}\right) & cov\left(\mathrm{X}^{'}, \mathrm{Y}^{'}\right) \\ cov\left(\mathrm{Y}^{'}, \mathrm{X}^{'}\right) & cov\left(\mathrm{Y}^{'}, \mathrm{Y}^{'}\right) \end{pmatrix} \tag{20}$$

The eigenvalues of M_{cov} is λ_1 and λ_2, and the corresponding eigenvectors are $\overrightarrow{v_1}$ and $\overrightarrow{v_2}$. The corresponding

eigenvector $\overrightarrow{v_s}$ of larger eigenvalue in λ_1 and λ_2 is the direction of maximum pose tracking error.

The eigenvalues of M_{cov} is λ_1 and λ_2, and the corresponding eigenvectors are $\overrightarrow{v_1}$ and $\overrightarrow{v_2}$. The corresponding eigenvector $\overrightarrow{v_s}$ of larger eigenvalue in λ_1 and λ_2 is the direction of maximum pose tracking error.

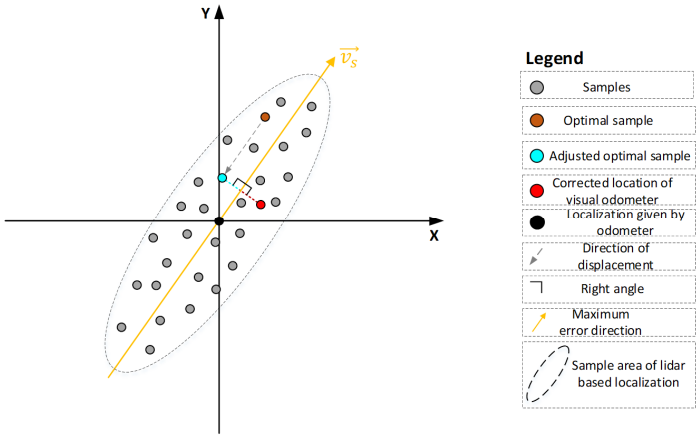

Fig.2. Maximum error direction compensation

As shown in Fig.2, the correction displacement of visual odometer relative to odometer will reduce the correction error of LIDAR in the direction of maximum error. T_{vo} reduce to one dimension on the projection of $\overrightarrow{v_s}$. The value D_{proj} of the projection point is:

$$D_{proj} = \overrightarrow{v_s} \cdot T_{vo} \tag{21}$$

The optimal sample P_{best} will be optimized along $\overrightarrow{v_s}$. After optimization, the pose is $\overline{P}_{best} = \left(\bar{x}_{best}, \bar{y}_{best}, \theta_{best}\right)^T$. The displacement correction $\overline{T}_{best} = \left(\bar{x}_{best}, \bar{y}_{best}\right)^T$ satisfies:

$$\begin{cases} D_{proj} = \overrightarrow{v_s} \cdot \overline{T}_{best} \\ \dfrac{\overline{T}_{best} - T_{best}}{\left\|\overline{T}_{best} - T_{best}\right\|} = \pm \dfrac{\overrightarrow{v_s}}{\left\|\overrightarrow{v_s}\right\|} \end{cases} \tag{22}$$

The robot pose P_t at time t can be achieved through adding the optimized pose $\overline{P}_{best}$ to P_{odom}:

$$P_t = P_{odom} + \overline{P}_{best} \tag{23}$$

IV. Experiment

The system setup can be seen in Fig.3. The LIDAR is SICK TIM551 and the visual sensor is Kinect. A laptop with Robot Operating System (ROS) is used to control the robot. The data of the robot is transmitted back to the laptop by a wireless route to monitor the state of the robot. The functions of Leica Tracker (AT960) and T-MAC are to record the exact pose of the robot and to evaluate the performance of the algorithm.

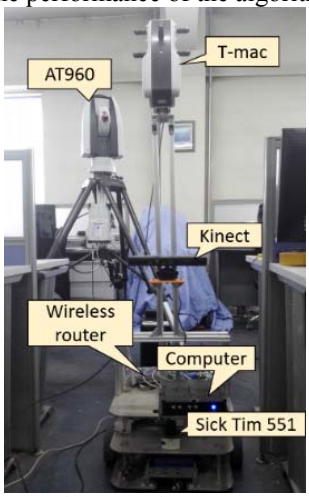

Fig.3. Experiment setup

A. Performance test of visual odometer and sample analysis of LBPT

Initial condition:

In the pose tracking test, the robot is placed in a narrow aisle and remains static. In the experiment, the robot needs to pass through all three aisles in turn.

Analysis of experimental process:

Visual odometer and scan matching based pose tracking algorithm continuously track the pose of the robot. T-MAC measurement system measures the pose of the robot.

Fig.4 shows the pose tracking process of the robot in the visual interface. The map points in the camera coordinate system of visual odometer are represented by red dots, the map points in the local map are represented by blue dots, and the LIDAR dots are represented by green dots.

Analysis of experimental results:

Table 1 introduces statistical indicators to quantitatively analyse the pose tracking errors on X axis and Y axis and updating time of visual odometer. In the whole pose tracking process, the LBPT traced the robot pose 30 times. Fig.5 introduces box chart analysis to obtain the extreme value, upper and lower quartiles, and median of sample score distribution during the normal operation of LBPT, which provides the statistical basis for VOAPT. Threshold settings in (29) are as follows: V_{th1}=10，V_{th2}=15，V_{th3}=0.7

Table 1

Visual odometer error statistical index

Statistical indicators	Mean	Medium	Standard deviation	Maximum deviation
X-axis deviation	0.050(m)	0.041(m)	0.042(m)	0.149(m)
Y-axis deviation	0.045(m)	0.035(m)	0.036(m)	0.130(m)
Computational time	40.3(ms)	41(ms)	6.2(ms)	-

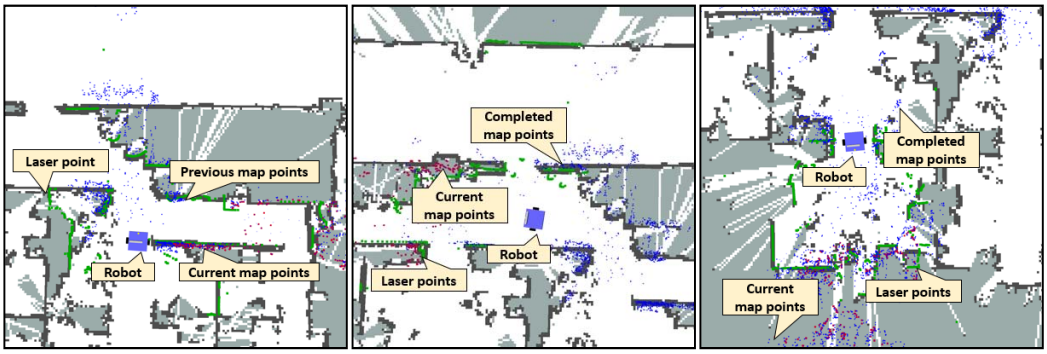

(a)Robot in 1st aisle in RVIZ (b)Robot in 2nd aisle in RVIZ (c)Robot in 3rd aisle in RVIZ

Fig.4. Robot navigation process in RVIZ

Table II

Pose tracking evaluation index of LBPT and visual odometer

(a)Evaluation index of LBPT

Evaluation index	value
μ_{lo}	0.0228(m)
σ_{lo}	0.0319(m)
UCL_{lo}	0.1184(m)
LCL_{lo}	0(m)

(b) Evaluation index of visual odometer

Evaluation index	value
μ_{vo}	0.0288(m)
σ_{vo}	0.0332(m)
UCL_{vo}	0.1283(m)
LCL_{vo}	0(m)

When both the visual odometer and the LBPT algorithm are running normally, the correction of the odometer results is shown in Fig.5. Considering the distribution of the sample score and the difference of the correction, the threshold values of each parameter in the credibility criteria T_s are shown in Table 2. The pose tracking results conforming to T_s show that the results of laser pose tracking are credible, otherwise the result is incredible. The algorithm needs to further determine the direction of maximum error and correct the pose tracking results in the direction by using the result of visual odometer

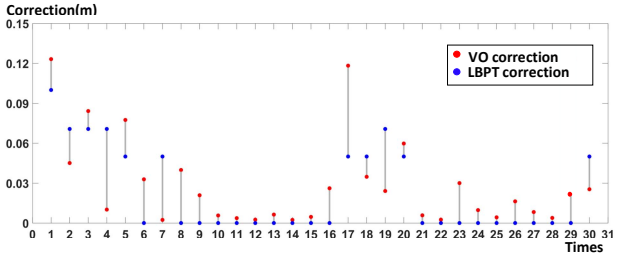

Fig.5. The correction of visual odometer and LBPT

B. VOAPT pose tracking test

Initial condition:

The environment is a long straight corridor with a certain degree of occlusion. The radial features are two pillars, two walls and a fire hydrant which provide enough reference information for pose tracking. The occlusion of the radial feature is an umbrella that blocked a pillar. When a large number of radial features are blocked, the pose tracking results would be inaccurate for LBPT, and the uncertain direction is along the corridor's axial direction.

Analysis of the experimental process:

The process of VOAPT is shown in Fig.6. As shown in Fig.6(a), the LIDAR was able to detect the 1st pillar and the fire hydrant, the distribution of sample score met the C_s. As the robot moving forward, the first pillar and the fire hydrant gradually left the detectable region, as shown in Fig.6(b). The distribution of sample score didn't meet the C_s. The result of visual odometer was used to compensate the error. As the robot moved forward, the 1st wall, 2nd wall and 2nd pillar gradually entered the LIDAR's detection area, the LBPT was able to give back credible result.

Analysis of experimental results:

The statistical indicators used to represent errors are: maximum error, average error, median error, and standard deviation of error, which is given in Table III.

Table III

Error analysis of LBPT and VOAPT

Statistical index	Maximum	Average	Medium	Standard deviation
LBPT X-axis error	1.060(m)	0.332(m)	0.153(m)	0.357(m)
VOAPT X-axis error	0.148(m)	0.045(m)	0.047(m)	0.029(m)
LBPT Y-axis error	0.302(m)	0.114(m)	0.067(m)	0.099(m)
VOAPT Y-axis error	0.133(m)	0.045(m)	0.036(m)	0.036(m)

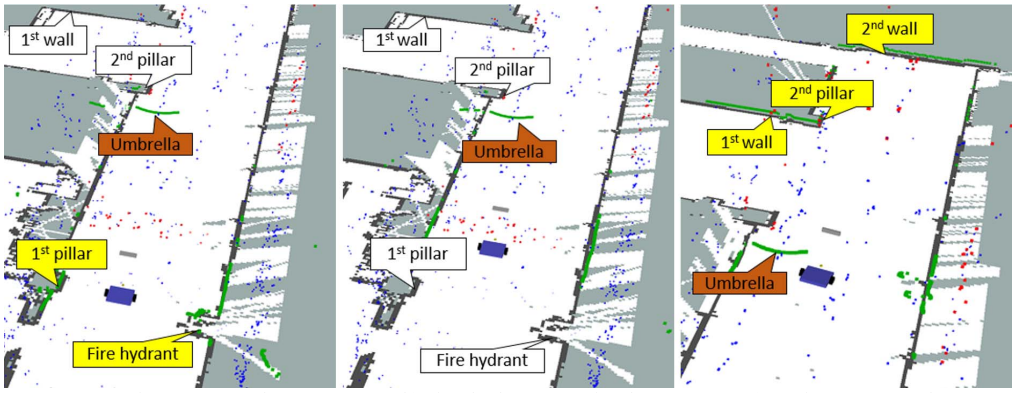

(a)Using LIDAR only (b)Visual odometer assisted (c) Using LIDAR only

Fig.6. The pose tracking process of VOAPT in RVIZ

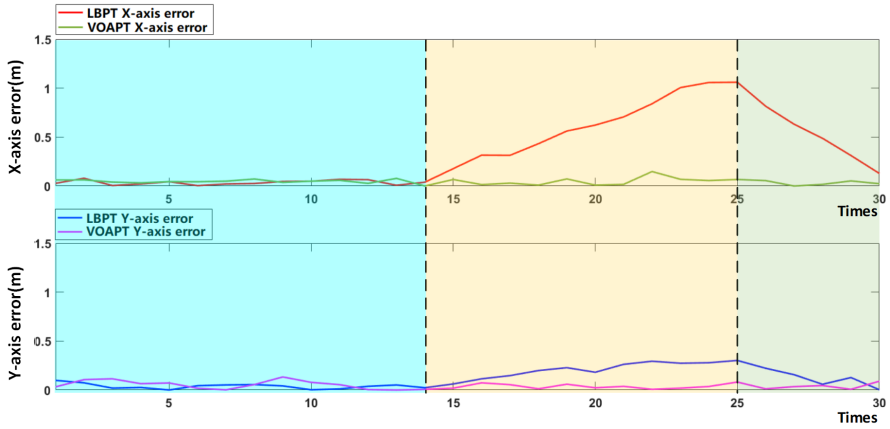

Fig.7 The error analysis of LBPT and VOAPT pose tracking

V. Conclusion

In this paper, VOAPT method is used to increase the robustness of pose tracking when the environment is blocked by obstacles. The method adopts visual odometer to provide extra information for pose tracking. By analysing and evaluating the score distribution of LBPT samples in an information-rich environment, the criteria for judging whether the LBPT is normal or not can be obtained. When the result is abnormal, it is necessary to find out the maximum error direction, and add the information of visual odometer to control and compensate the error in this direction to a certain extent. The result shows that VOAPT can make pose tracking more reliable..

References

[1] Jung, Minkuk, and J. B. Song. "Efficient autonomous global localization for service robots using dual laser scanners and rotational motion." International Journal of Control, Automation and Systems 15.2(2017):743-751.

[2] Chen, Shu , et al. "3D Pose Tracking with Multi-Template Warping and SIFT Correspondences." IEEE Transactions on Circuits and Systems for Video Technology 26.99(2015): 2043-2055.

[3] Zhuang, Zhang , et al. "Scale Estimation and Correction of the Monocular Simultaneous Localization and Mapping (SLAM) Based on Fusion of 1D Laser Range Finder and Vision Data." Sensors 18.6(2018):1948-1960.

[4] Hidalgo, C, C. Saripalli, and H. L. Granzier. "An autonomous mobile robot with a 3D laser range finder for 3D exploration and digitalization of indoor environments." Robotics & Autonomous Systems 45.3–4(2003):181-198.

[5] Scaramuzza, D, and F. Fraundorfer. "Visual Odometry" Robotics & Automation Magazine IEEE 18.4 (2011): 80-92.

[6] Li, Hao , F. Nashashibi , et al. "Localization for intelligent vehicle by fusing mono-camera, low-cost GPS and map data." Intelligent Transportation Systems (ITSC), 2010 13th International IEEE Conference on IEEE, 2010.

[7] Fox, Dieter , et al. "Monte Carlo Localization: Efficient Position Estimation for Mobile Robots." Proceedings of the Sixteenth National Conference on Artificial Intelligence and Eleventh Conference on Innovative Applications of Artificial Intelligence, 1999.

[8] Thrun S, Burgard W, Fox D. A Probabilistic Approach to Concurrent Mapping and Localization for Mobile Robots[J]. Autonomous Robots, 31.3 (1998): 29-53.

[9] Chien, Chiang Heng , et al. "Enhanced Monte Carlo localization incorporating a mechanism for preventing premature convergence." Robotica (2016): 1504-1522.

[10]Rupeng, Y., Fuhai, Z., Qujia D., Guozhi, L., Yili, F "An enhanced pose tracking method using progressive scan matching." Industrial Robot, Vol. 46.2(2019):235-246.

[11] Mei, Qiaozhu , D. Zhang , and C. X. Zhai . "A general optimization framework for smoothing language models on graph structures." International Acm Sigir Conference on Research & Development in Information Retrieval ACM, 2008.

[12]MLA Kaess, Michael. "Incremental smoothing and mapping." IEEE Transactions on Robotics 24.6(2008):1365-1378.

[13]Klein, Georg , and D. Murray . "Parallel Tracking and Mapping for Small AR Workspaces." Mixed and Augmented Reality, 2007. ISMAR 2007. 6th IEEE and ACM International Symposium on ACM, 2007.

[14]Newcombe, Richard A. , S. J. Lovegrove , and A. J. Davison . "DTAM: Dense tracking and mapping in real-time." IEEE International Conference on Computer Vision, ICCV 2011, Barcelona, Spain, November 6-13, 2011 IEEE, 2011.

[15]Engel, Jakob , V. Koltun , and D. Cremers . "Direct Sparse Odometry." IEEE Transactions on Pattern Analysis and Machine Intelligence (2017):14-27.